Earth and Planetary Science Letters 522 (2019) 125–134

Contents lists available at ScienceDirect

Earth and Planetary Science Letters

www.elsevier.com/locate/epsl

Eastern North American climate in phase with fall insolation throughout the last three glacial-interglacial cycles

Hai Cheng [a,b], Gregory S. Springer [c,*], Ashish Sinha [d], Benjamin F. Hardt [e], Liang Yi [f], Hanying Li [a], Ye Tian [a], Xianglei Li [a], Harold D. Rowe [g], Gayatri Kathayat [a], Youfeng Ning [a], R. Lawrence Edwards [b]

[a] Institute of Global Environmental Change, Xi'an Jiaotong University, China
[b] Department of Earth Sciences, University of Minnesota, USA
[c] Department of Geological Sciences, Ohio University, USA
[d] Department of Earth Science, California State University Dominguez Hills, USA
[e] Department of Earth, Atmospheric and Planetary Sciences, Massachusetts Institute of Technology, USA
[f] State Key Laboratory of Marine Geology, Tongji University, China
[g] Bureau of Economic Geology, University of Texas at Austin, USA

ARTICLE INFO

Article history:
Received 21 December 2018
Received in revised form 1 June 2019
Accepted 20 June 2019
Available online 9 July 2019
Editor: I. Halevy

Keywords:
isotope geochemistry
U-series chronology
paleoclimate
North America
Pleistocene

ABSTRACT

The nature and controls of orbital-scale climate variability in North America (NA) are subjects of ongoing debates. On the basis of previous cave records from Southwestern United States, two mutually incompatible hypotheses have been proposed. One links NA orbital-scale climate variability to Northern Hemisphere (NH) summer insolation forcing in a manner analogous to low-latitude monsoon systems, while the other suggests that it is not causally tied to either changes in global ice-volumes or NH summer insolation. Here we report new cave oxygen isotope ($\delta^{18}O$) records from Buckeye Creek Cave (BCC), West Virginia, east central North America, covering most of the past three glacial-interglacial periods (~335 to 45 kyr ago). The BCC $\delta^{18}O$ record exhibits a strong precession-band cycle, which is in-phase with changes in global ice-volumes (i.e., sea level), sea surface temperatures in the NE Gulf of Mexico and is consistent with the results from published cave records from Nevada and Devils Hole. As with global ice-volume, the BCC records lag summer insolation at 65°N by ~5000 yr, which stands in contrast with records of low-latitude monsoon variability in South America and Asia, which are in phase and out-of-phase with changes in summer insolation and sea level, respectively. Provided the degree of lag to summer insolation provides a measure of competing forcing from global ice-volume and summer insolation, our data suggest that NA orbital-scale climate variability is dominantly driven by ice-volume forcing. In addition, the sea surface temperatures in the NE Gulf of Mexico and changes in northern high-latitude cryosphere may be also important in explaining the unusually low $\delta^{18}O$ values at times of the intermediate ice-volume periods in BCC and other NA cave records.

1. Introduction

The Quaternary glacial-interglacial cycles and the accompanying climate changes in much of the Earth's climate systems are ultimately governed by changes in Earth's orbital geometry (Imbrie et al., 1984). Strictly, this orbital (or astronomical) theory of climate change posits that mid-summer changes in Northern Hemisphere summer insolation (NHSI) at latitude 65°N drive variances in ice sheets extent (global ice-volume) at the periods of orbital tilt and precession (i.e., classic Milankovitch Theory), which in turn, incite ancillary changes in other parts of the global climate systems via various forcing and feedback mechanisms (Ruddiman, 2006). The Milankovitch Theory (both in the strict and broader sense) is well supported by a substantial body of largely consistent paleoclimate data from marine and terrestrial sediments (e.g., Imbrie et al., 1984; An et al., 2011; Spratt and Lisiecki, 2016), polar ice cores (e.g., Jouzel et al., 2007; Bereiter et al., 2015) and cave deposits (e.g., Cruz et al., 2005; Cheng et al., 2012, 2013a, 2016a).

While the orbital-forcing is particularly well characterized at the low latitude (e.g., inter-hemispheric monsoon systems) and high latitude climate systems, much less is known about the orbital-scale changes in the mid-latitudes continental climate be-

* Corresponding author.
E-mail address: springeg@ohio.edu (G.S. Springer).

https://doi.org/10.1016/j.epsl.2019.06.029
0012-821X/

cause few records have requisite chronological constraints and temporal resolution to allow a precise comparison with orbital-scale climate variations over several ice-age cycles. This is particularly the case for the mid-latitude regions of North America (NA), where a large body of proxy and geomorphic evidence point to the occurrence of large hydroclimatic changes, personified for example by dramatic changes in lake levels in the western NA, on millennial to orbital timescales (e.g., Grayson, 2011; Wendt et al., 2018). Notwithstanding, the temporal patterns of these large-scale hydroclimate shifts and their linkage to orbital forcing remains a contentious issue. Results from other speleothem records from the region (Great Basin, Fig. 1) including updated and new records from the Devils Hole (Moseley et al., 2016; Wendt et al., 2018) however, suggest that the southwestern NA climate variability was linearly forced by NHSI over the last 350,000 yr, matching in phase and amplitudes the mid-summer NHSI at 65°N (Lachniet et al., 2011, 2014; Moseley et al., 2016; Wendt et al., 2018). However, a more recent phasing analysis of the Great Basin speleothem records indicates that southwestern NA climate variability exhibited variable lags (−900 to 6600 yr) to NHSI over the last two glacial cycles in the precession band (Lachniet et al., 2017).

Previously, it has been hypothesized that climate variability in ice-sheet-proximal regions in the Northern Hemisphere should be sensitive to delayed ice-volume signals, which would get transferred to nearby oceans and landmasses via atmospheric dynamics (Ruddiman, 2006) – a scenario in accordance with the strict definition of Milankovitch Theory. In contrast, the mid and low latitude climate systems should be sensitive to direct in-phase mid-summer insolation forcing. These contrasting responses at ice-sheet proximal and distant regions have been characterized as 'late' (those that lie near that of the slow-responding ice sheets with precession phase around September insolation) or 'early' (i.e., those responses close to that of NHSI ∼July insolation phase in the precession band) climate responses, respectively. Indeed, the latter is clearly attested by proxy records from Asian and South American monsoon systems (e.g., Cruz et al., 2005; Wang et al., 2007; Cheng et al., 2012, 2016a) and mid-latitude westerly west-central Asia (Cheng et al., 2012, 2016b). As for the former, one would therefore expect that orbital-scale variability in NA, being proximal to ice-sheets (Fig. 1), should exhibit in-phase response to changes in ice-volume and thus a ∼5 kyr lag to NHSI in precession band (Ruddiman, 2006).

To date, no single record from outside southwestern NA exists that spans multiple ice-age cycles while being both high-resolution and absolutely dated. In this paper, we assess the orbital-scale variability of NA climate over multiple ice-age cycles by using a high-resolution and absolutely dated ∼290 kyr-long cave climate record from Buckeye Creek Cave, West Virginia, east-central NA (ECNA) (Figs. 1–2). The long duration and geographic location of our record together with regional and global datasets allow us to characterize the orbital-scale pattern of hydroclimate variability. Our ECNA climate record displays significant precession variance that has direct bearing on the question regarding the precession phase and in turn whether the climate variations are dominantly controlled by changes in ice-volume or NHSI on mid-latitude NA climates.

2. Samples and methods

2.1. Buckeye Creek Cave and speleothems

Buckeye Creek Cave (BCC) is located in the Buckeye Creek (BC) watershed (14 km^2) of southeastern West Virginia, USA (37°58′N, 80°24′W, 600 m above sea level) (Fig. 1). Calcite stalagmites

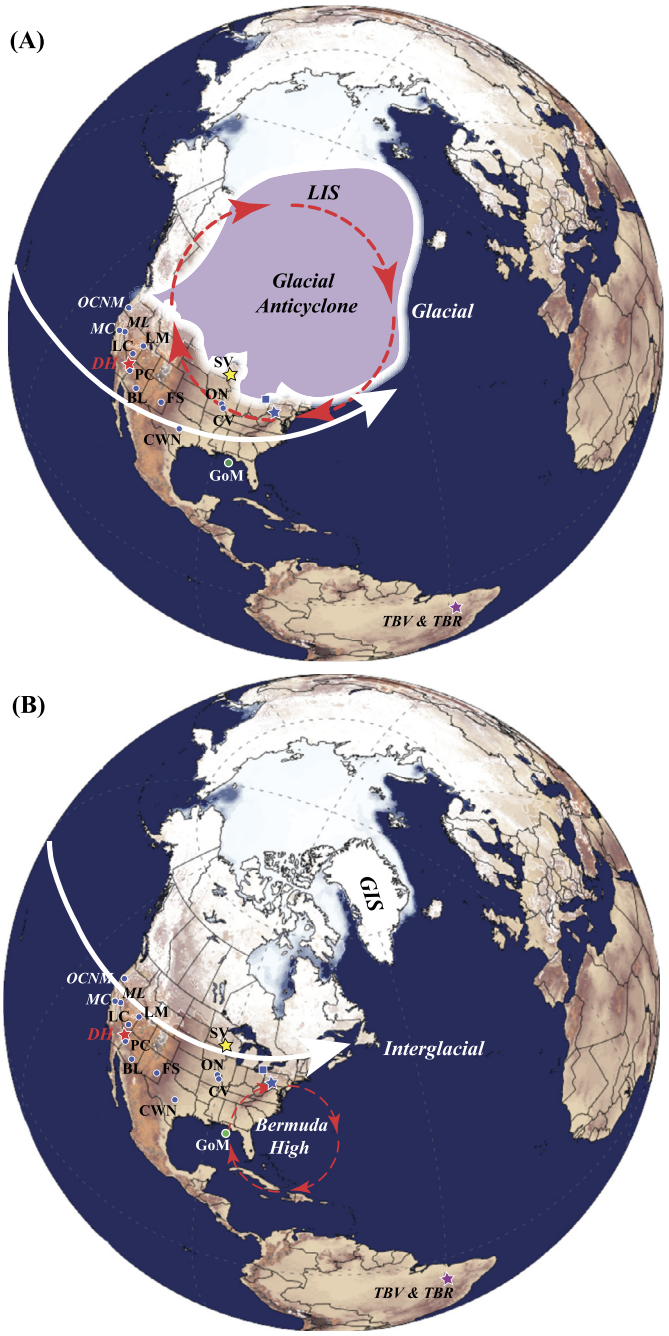

Fig. 1. Locations of cave and ice sheet. **(A)** Schematic map of glacial period. White area: the farthest extent of the Laurentide Ice Sheet (LIS) during the last glacial. Blue star: Buckeye Creek Cave. Red star: Devils Hole (DH). White stars: Cave of the Bells (COB), Fort Stanton (FS), Cave without a Name is CWN, Moaning and McLean (MC/ML), Oregon cave (OCNM), Lehman (LM), Leviathan (LC), Pinnacle (PC), Onondaga (ON), Crevice (CV), Spring Valley (SV) caves. Blue square: the location of a GNIP station, Coshocton, OH. Yellow arrow: Polar-Jet. Orange arrows: Glacial Anticyclone (COHMAP Members, 1988). **(B)** Schematic map of interglacial period. Similar to **(A)**, except the orange arrows show the Bermuda High, and the white area shows Greenland ice sheet. During the cold (warm) mode, the polar jet stream shifts southward (northward), leading to more (less) moisture derived from Pacific Ocean in southern (northern) US, resulting in lighter (heavier) δ^{18}O of precipitation in the region. While the Fort Stanton record in south and Spring Valley record in north show opposite precipitation δ^{18}O excursions across the cold and warm modes, the amplitude of BCC record in-between is virtually mute. (For interpretation of the colors in the figure(s), the reader is referred to the web version of this article.)

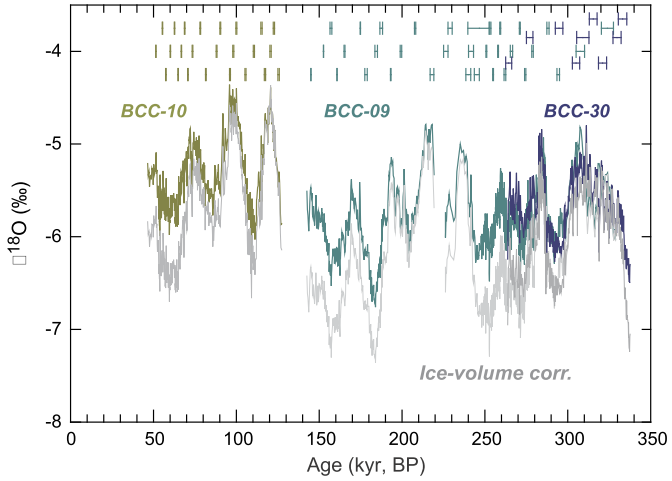

Fig. 2. BCC $\delta^{18}O$ time series. The BCC record is composed from three samples: BCC-10 (olive), BCC-09 (teal) and BCC-30 (dark blue). Horizontal error bars are ^{230}Th dating results (2σ) and color-coded. The grey curves are the BCC records after correction for ice-volume effect using the sea level dataset of Spratt and Lisiecki (2016).

BCC-08, -09, and -10 were collected in 2004 and BCC-30 was collected in 2016. The stalagmites were collected from dry upper level passages about 1 km downstream of the cave entrance. We previously provided an analysis of stable carbon isotopic values ($\delta^{13}C_c$) in BCC-10 and its partial replicate BCC-08 (Springer et al., 2014) and herein we interpret stable oxygen isotopic values ($\delta^{18}O_c$) values from BCC-10 together with previously unpublished data from stalagmite BCC-09 and its partial replicate BCC-30. The latter two stalagmites are ~80 and 36 cm tall with diameters of ~8.5 and 7.5 cm, respectively (Fig. S1). Today, the cave site is forested under a humid and temperate climate with a typical mid-latitude seasonality. Mean annual temperature and precipitation are ~10 °C and 1130 mm, respectively. The detailed cave settings are described in Hardt et al. (2010) and Springer et al. (2008, 2014).

2.2. ^{230}Th dating

All U/Th ages were obtained by using a recently improved dating technique (Cheng et al., 2013a), on inductively coupled plasma mass spectrometers at the University of Minnesota (Neptune, BCC-09 and BCC-10) and Xi'an Jiaotong University (Neptune-Plus, BCC-30), respectively. The U and Th isotope ratios are measured by multi-collector inductively coupled plasma mass spectrometers (MC-ICP-MS). We use standard chemistry procedures to separate uranium and thorium for dating (Edwards et al., 1987). A triple-spike (^{229}Th–^{233}U–^{236}U) isotope dilution method was employed to correct for instrumental fractionation and determine U/Th isotopic ratios and concentrations. The instrumentation, standardization and half-lives are reported in Cheng et al. (2013a). All U/Th isotopes were measured on a MasCom multiplier behind the retarding potential quadrupole in the peak-jumping mode. Uncertainties in U/Th isotopic data were calculated offline at 2σ level, including corrections for blanks, multiplier dark noise, abundance sensitivity, and contents of the same nuclides in spike solution. Corrected ^{230}Th ages assume the initial $^{230}Th/^{232}Th$ atomic ratio of $4.4 \pm 2.2 \times 10^{-6}$, the values for a material at secular equilibrium with the bulk earth $^{232}Th/^{238}U$ value of 3.8. The age corrections are trivial due to high $^{230}Th/^{232}Th$ ratios. The U decay constants are reported in Cheng et al. (2013a).

All ages are in stratigraphic order within dating uncertainties (Fig. S2). Age models were constructed based on U/Th age constraints using cubic splines in *clam* (Blaauw, 2010) for BCC-09 and BCC-10. Linear interpolation was used between adjacent dates for BCC-30 because the record is shorter and lacks gaps (Fig. S2). All the U/Th dating results are listed in Supplemental Tables S1-3 (BCC-09, BCC-10, BCC-30, respectively).

2.3. Stable isotope measurements

$\delta^{18}O_c$ samples were milled at 1-mm (BCC-09) and 0.5-mm (BCC-10) intervals along the vertical growth axis and analyzed using a GasBench II coupled to a Thermo-Finnigan Delta-Plus XP IRMS at the University of Kentucky in Lexington. Samples of BCC-30 were milled at 1 mm interval and analyzed using a Kiel-IV device coupled to MAT253 in Xi'an Jiaotong University. Overall $\delta^{18}O_c$ measurements have a temporal resolution of between 200 and 70 yr (average of ~120 yr). Results are reported in per mil (‰), relative to the Vienna PeeDee Belemnite (VPDB). Standard measurements have an analytical precision (1σ) of typically 0.08‰ in both laboratories. All $\delta^{18}O_c$ data are provided in Supplemental Table S4, including uncorrected and ice-volume corrected values.

BCC-09 and BCC-30 were separated by 50-m prior to collection and their replication of contemporaneous $\delta^{18}O_c$ time series (the replication test, Hendy, 1971) (Fig. 2) suggests they must have been equally affected by above- and in-cave factors controlling oxygen isotopic fractionation. On the other hand, consistent offsets are unlikely because each stalagmite-precipitating drip-water has a unique combination of flow path, CO_2 partial pressure, residence time, solute concentration, degassing history etcetera. Thus, replicated BCC records strongly suggest that their overall $\delta^{18}O_c$ variability is related to a common major factor, the $\delta^{18}O$ of precipitation ($\delta^{18}O_p$), instead of other additional processes.

2.4. Statistics analyses

Correlation coefficients between different records are obtained using the bootstrap resampling method in MATLAB R2014a. The total resampling performance is 2000, which provides a significance level (p) of <0.05 for the expectation of correlation coefficient. The red curves in figures are the probability density curves fitted by the Gaussian distribution. Correlation coefficients are labeled together with standard errors. Three ranges of these correlation coefficients (shadow areas in the figures) generally do not cross origin points, further demonstrating their statistical significances. We also calculate the Pearson correlation coefficients (r) for the paired datasets. All of them are close to the expectations labeled in the figures with statistical significances at $p < 0.05$ level as indicated in figure captions.

In order to identify periodic components in the spectrum of climate records, we applied the spectral analysis using the REDFIT38 software (Schulz and Mudelsee, 2002) with Lomb-Scargle Fourier transform and Welch's Overlapped Sequence Averaging procedure. First-order autoregressive (AR1) time series are produced to match input climate data. χ^2-distribution is performed to assess the statistical significance of a spectral peak. Cross-spectrum analysis results are obtained using the ARAND software package. Detailed methods are described in Howell et al. (2006).

3. Proxy interpretation

We previously demonstrated that BCC $\delta^{18}O_c$ values vary in response to $\delta^{18}O_p$, which is locally determined by season and moisture source/trajectory (Fig. 3): summer rainfall originated from the Gulf of Mexico (GoM) exhibits heavier $\delta^{18}O_p$ values than during other times of the year (Hardt et al., 2010) (Fig. 1B). Based on analysis of modern $\delta^{18}O_p$ values at the nearest station of the Global Network of Isotopes in Precipitation at Coshocton, OH (IAEA/WMO, 2006), temperature and the total amount of precipi-

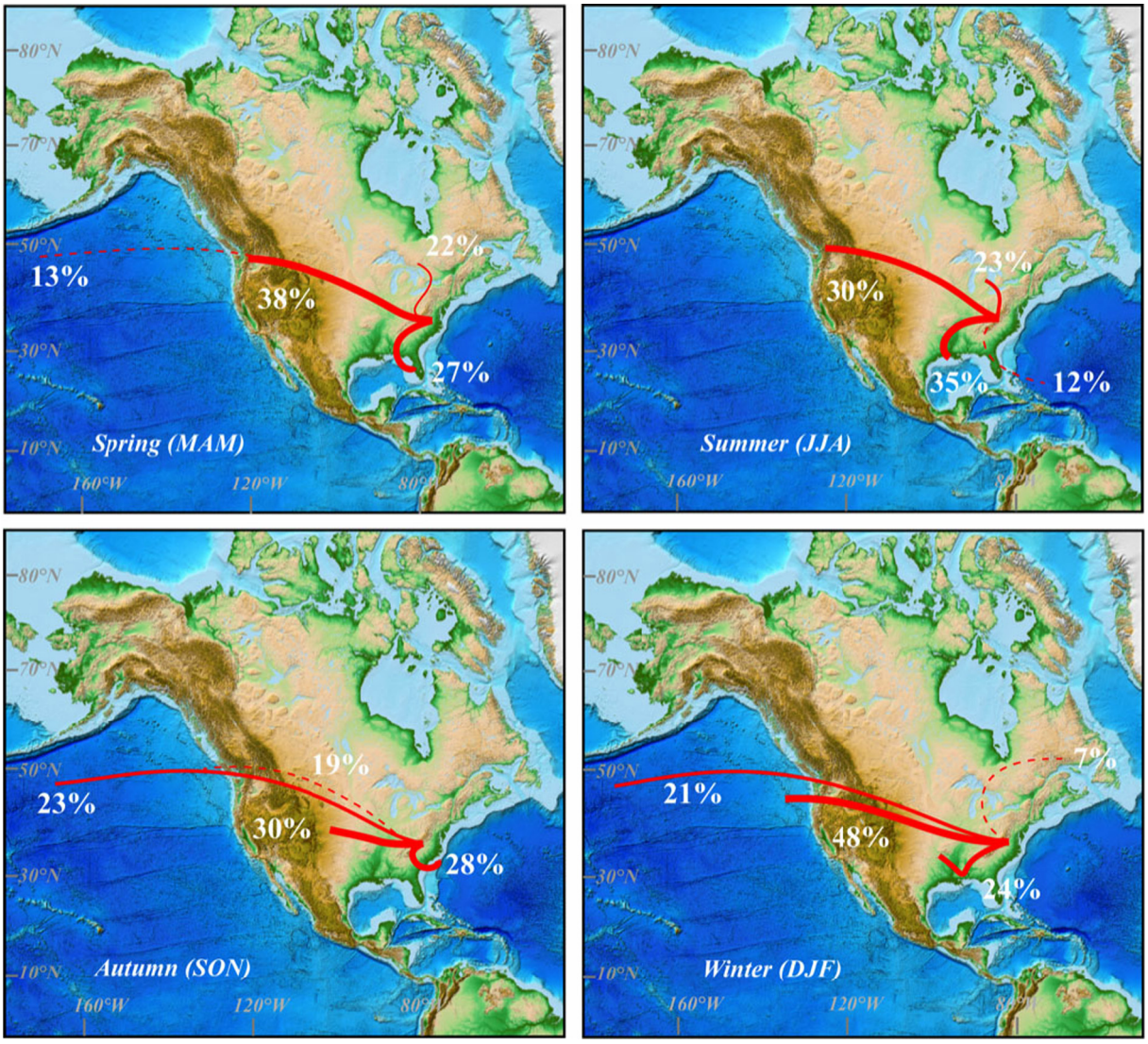

Fig. 3. Seasonal variance of air parcel trajectories to BCC site. The trajectory analysis results for BCC location are obtained using TrajStat (Wang et al., 2009), a free software plugin of MeteoInfo software (Wang, 2014), combined with trajectory calculation module of HYSPLIT (Draxler and Hess, 1998). Detailed methods are described in TrajStat Help documentation. Monthly NCEP/NCAR reanalysis meteorological datasets from 1966 to 1976 are obtained from website ftp://arlftp.arlhq.noaa.gov/pub/archives/reanalysis. We computed backward (120 h) (sampled four times daily at UTC 00, 06, 12 and 18) trajectory ensembles and clusters of four seasons (DJF, MAM, JJA, SON) respectively, which initialized at 1500 m above ground level (corresponding to ~850 hPa).

tation are less likely to provide a strong control on $\delta^{18}O_c$ (Hardt et al., 2010). $\delta^{18}O_p$ and temperature at Coshocton exhibit a significant correlation ($p < 0.001$) based on monthly measurements, but with a slope of only +0.27‰/°C, far less than what has been observed in multi-station analyses (Rozanski et al., 1993; Yurtsever, 1975). It is unlikely that temperature provides a substantial role in determining modern $\delta^{18}O_c$ values because oxygen isotope fractionation between water and calcite is of similar magnitude but opposite sign (−0.24‰/°C) (Kim and O'Neil, 1997). The cave $\delta^{18}O_c$ record is also a function of changes in seawater $\delta^{18}O$ ($\delta^{18}O_{sw}$), which is enriched (depleted) during periods of ice sheet expansion (retreat). Therefore, the true signal in our record would be approximately 1‰ larger than what is recorded by the speleothems. To first order, we removed this seawater effect from our BCC records on the basis of a recent stacked sea level dataset (Spratt and Lisiecki, 2016) (Fig. 2).

Coshocton precipitation totals exhibit a statistically non-significant positive correlation ($p = 0.78$) with $\delta^{18}O_p$, the opposite relationship predicted by the 'amount effect' (Hardt et al., 2010). Therefore, we follow the reasoning in our previous study (Hardt et al., 2010), to interpret cave $\delta^{18}O_c$ as reflecting changes in the annual balance of precipitation between summer and winter. Analysis of the seasonal variability of the moisture trajectory in the cave site support our interpretation: during the warm period of the year (late spring to early autumn), significant moisture in the site is derived from the GoM (Figs. 1B and 3A-C) or continent with heavier $\delta^{18}O_p$. Conversely, during the cold period of year (late autumn to next early spring), moisture derived mostly from Pacific with lighter $\delta^{18}O_p$ via the jet-stream (IAEA/WMO, 2006; Figs. 1B and 3D).

The moisture ratio between the warm and cold times may then be a dominant factor controlling mean annual $\delta^{18}O_p$ values via changing moisture source and trajectory (Figs. 1 and 3). More broadly, analogous to the seasonal variability, during a warm (cold) interglacial/interstadial (glacial/stadial) period, more (less) moisture from the Gulf of Mexico and less (more) moisture from the Pacific/continent may explain the observed higher (lower) $\delta^{18}O$ proxy values in the continental interior of NA, such as is observed in the modern due to seasonal differences in air parcel trajectories and moisture sources (Fig. 3). Conceptually, larger (smaller)

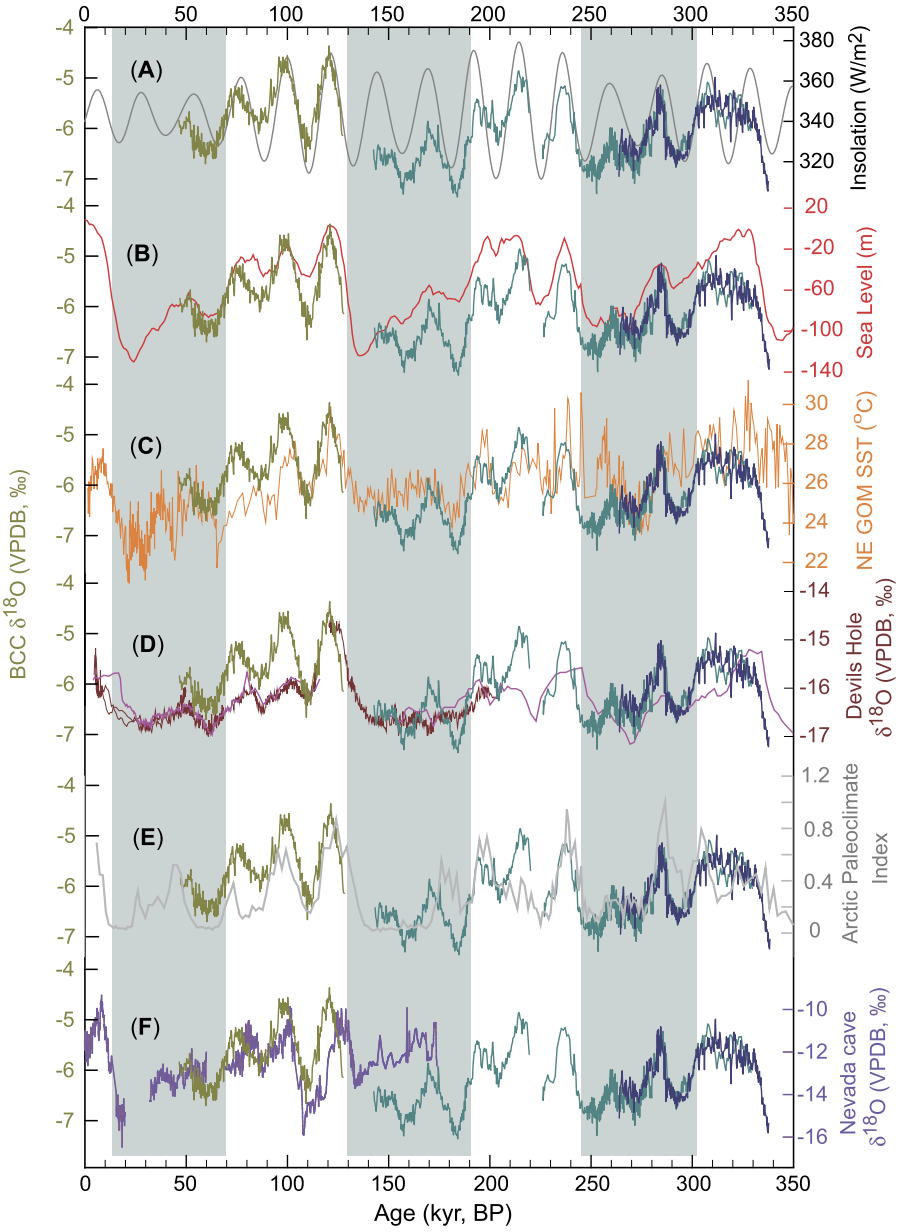

Fig. 4. Comparison of the BCC $\delta^{18}O$ records to other climate records. (**A**) BCC records (BCC-10, olive; BCC-09, teal; and BCC-30, dark blue) and September 21 insolation at 38°N (grey, Laskar et al., 2004). BCC records show strong precession cycles that are in-phase with September insolation changes. 38°N was chosen as it is the approximate latitude for our study site. (**B**) BCC records and sea level change (red, Spratt and Lisiecki, 2016). (**C**) BCC records and SST record from NE GoM (orange, Nürnberg et al., 2008). (**D**) BCC records and Devils Hole records (pink, Winograd et al., 2006 and dark red, Moseley et al., 2016). (**E**) BCC records and Arctic Paleoclimate Index (grey, Marzen et al., 2016). (**F**) BCC records and Nevada cave records (purple, Lachniet et al., 2014).

Laurentide Ice Sheet (Fig. 1A) would lead to stronger (weaker) glacial anticyclone over NA, lower (higher) GoM SST, and weaker (stronger) Bermuda High, resulting in less (more) moisture transported into NA continental interior from the GoM (Fig. 1B) (e.g., Peixóto and Oort, 1983), and thus heavier (lighter) $\delta^{18}O_p$ and in turn heavier (lighter) cave $\delta^{18}O_c$ values. This interpretation is consistent with a previous notion that explains the millennial-scale climate variability in southwestern USA (Asmerom et al., 2010; Wagner et al., 2010).

4. Results and discussion

4.1. Orbital-scale variability

The combined BCC $\delta^{18}O_c$ records have an overall amplitude of ~2‰ and cover approximately the past three glacial-interglacial periods, displaying prominent precession cycles (Figs. 2 and 4), which are in-phase and positively correlated with September 21 insolation at the latitude of BCC (38°N) (Fig. 5). Comparisons with other proxy records suggest the BCC records are remarkably similar to the sea level or global ice-volume (Fig. 6, $r = 0.70$, $p < 0.001$) (Spratt and Lisiecki, 2016), Devils Hole vein calcite $\delta^{18}O$ records (Moseley et al., 2016) (Fig. S3, $r = 0.58$, $p < 0.001$), sea surface temperature (SST) of Northeast GoM (Nürnberg et al., 2008) (Fig. S4, $r = 0.43$, $p < 0.001$), and the Arctic Paleoclimate Index (a sea ice proxy, Marzen et al., 2016) (Fig. S5, $r = 0.51$, $p < 0.001$). The BCC $\delta^{18}O_c$ records also correlate well with the portion (~70 to 127 kyr ago) of the Great Basin composite speleothem record on the "Leviathan chronology" (Fig. S6) (Lachniet et al., 2014), although the correlation with entire composite record is rather complicated possibly because of the significant (~3‰) latitude effect on the cave $\delta^{18}O_c$ values at three different cave locations and gaps in

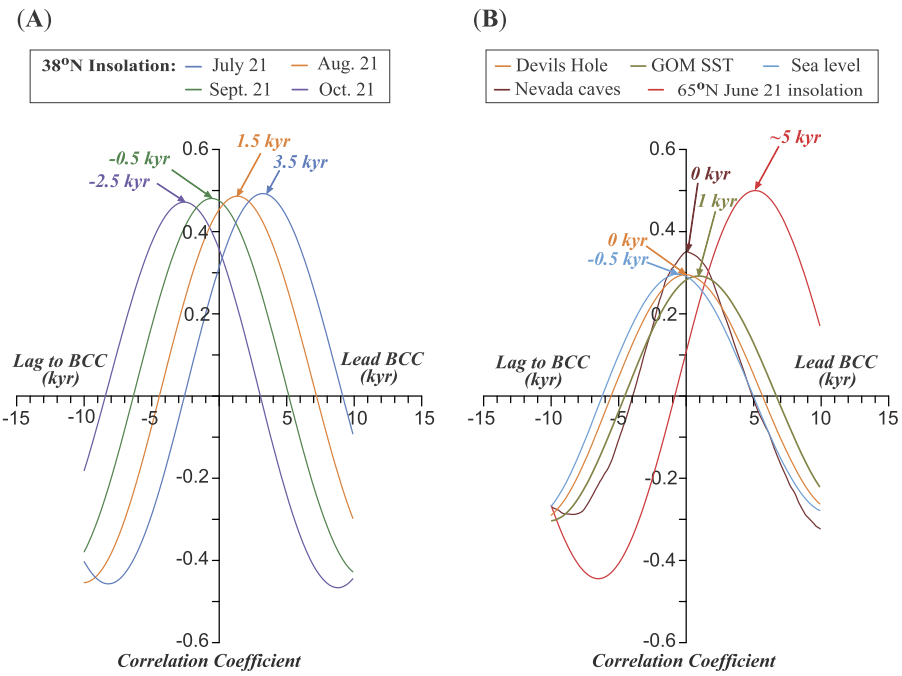

Fig. 5. Phase relation of BCC records with other records at precession band. (**A**) Cross-correlations were performed between linear interpolated BCC speleothem δ^{18}O records and local insolation. **(B)** The phase relations show the precession phase of BCC records relative to Devils Hole δ^{18}O (orange), GoM SST (olive), sea level (blue) and June 21 insolation at 65°N (Laskar et al., 2004) on precession band, respectively. The time series were linearly interpolated on common, even timescales.

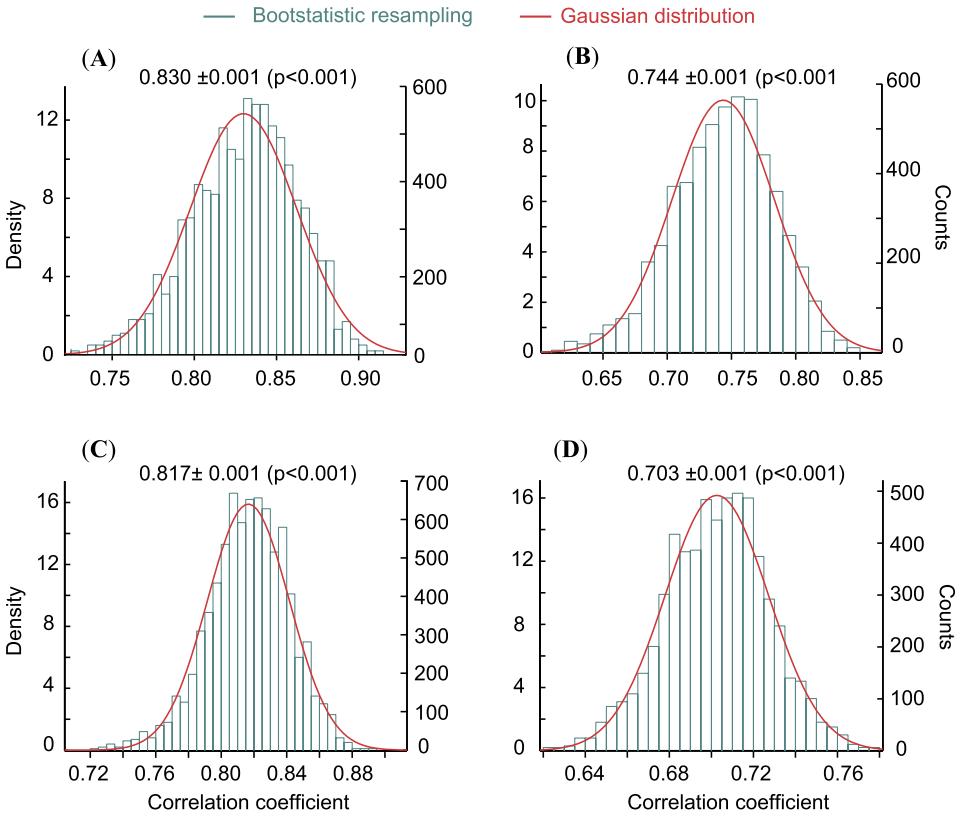

Fig. 6. Correlations of BCC records with sea level. Significant correlations of sea level (Spratt and Lisiecki, 2016) with BCC results. Sea level versus (**A**) BCC-10 ($r = 0.830$, $p < 0.001$), **(B)** BCC-09 ($r = 0.744$, $p < 0.001$), **(C)** BCC-30 ($r = 0.817$, $p < 0.001$) and **(D)** all BCC ($r = 0.703$, $p < 0.001$) records, respectively.

other portions of the record (Lachniet et al., 2014). Notably, all of aforementioned proxy records have significant powers in eccentricity (~100 kyr), obliquity (~41 kyr) and precession (~23 kyr) bands (Fig. 7).

The phase analysis of common and significant precession cycle among NHSI, sea level, cave records from NA, suggests that the BCC $\delta^{18}O_c$ record contains the most prominent precession variability (Fig. 7). The BCC record significantly lags NHSI and is

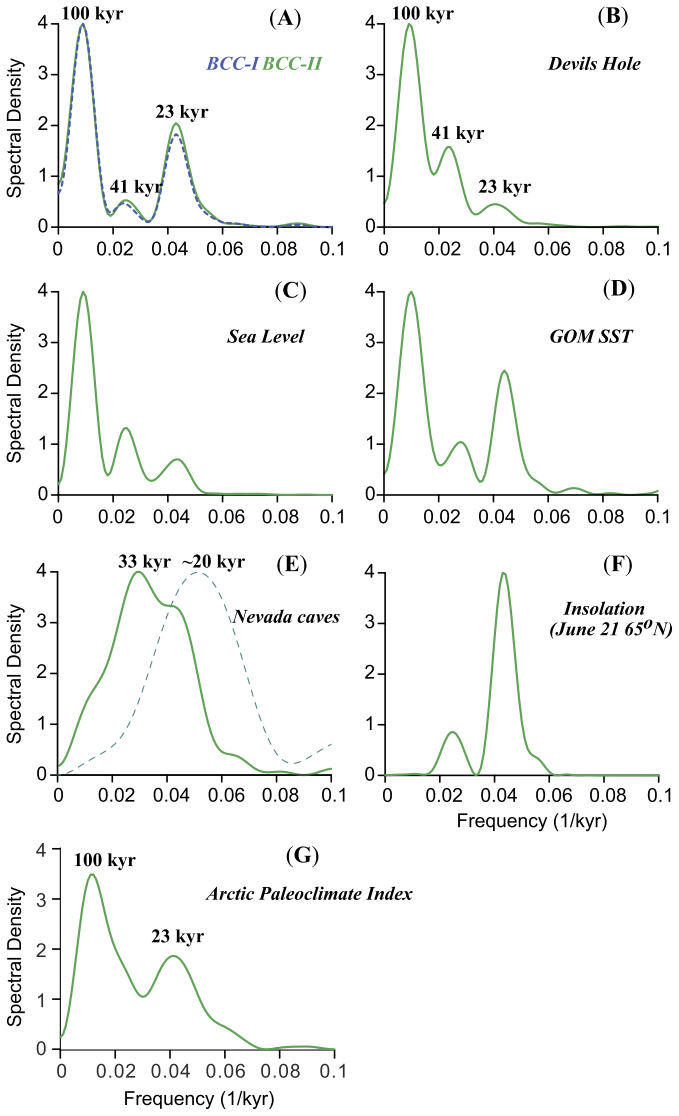

Fig. 7. Spectral analysis results of BCC and other records. **(A)** Spectral analysis results of BCC records. Green and blue dashed lines are obtained by mean value filling and data interpolating in the two gaps (127.7–141.5 and 219.5–226.3 ka), respectively. **(B–G)** Spectral analysis results of Devils Hole (Winograd et al., 2006; Moseley et al., 2016), sea level (Spratt and Lisiecki, 2016), SST of Gulf of Mexico (Nürnberg et al., 2008), Nevada caves (Lachniet et al., 2014), June 21 insolation at 65°N (Laskar et al., 2004), and Arctic Paleoclimate Index (Marzen et al., 2016).

broadly in-phase with September insolation with a phase angle of ∼80°, a ∼5 kyr lag, relative to June 21 insolation in the precession band (Fig. 5). Additionally, the Great Basin speleothem records also share the same phase within uncertainty and all significantly lag June 21 insolation by ∼5 kyr, which places them in-phase with both ice-volume and GoM SST records (Fig. 5B). Together these observations imply that the NA orbital-scale climate variability is consistent with the 'late response' mechanism (cf. Ruddiman, 2006). The aforementioned results from our absolute-dated BCC records are consistent with the SPECMAP marine $\delta^{18}O$ timescale, which was orbitally tuned and thus agrees with the ∼5 kyr lag predicted by Milankovitch Theory (Imbrie et al., 1984; Ruddiman, 2003). In precession band, our data independently supports Milankovitch Theory that NHSI variances drive changes in the NH ice-volume. Furthermore, our analysis also supports a hypothesis that precession-induced changes in summer insolation produce distinct climate variability in the ice-sheet proximal regions via the (delayed) ice-volume forcing (e.g., Ruddiman, 2006). Notably, while the large decreases of the BBC $\delta^{18}O_c$ at ∼110, 190 and 290 kyr BP are coherent with the increases (decrease) of the ice-volume (sea level) (Fig. 4B), regarding absolute value, these prominent low $\delta^{18}O_c$ excursions occurred at times of the intermediate ice-volume. Similar features were also noted in Nevada cave records (Lachniet et al., 2014, 2017). These observations cannot be simply attributed to the ice-volume forcing, and instead, a better explanation may involve changes in NE GoM SST (Nürnberg et al., 2008) and/or northern high-latitude sea ice (Marzen et al., 2016) (both correlating significantly with the BCC record, Figs. S4 and S5). In addition, the relatively low MIS 9 $\delta^{18}O_c$ value compared with ice-volume around 330 kyr BP in our records (Fig. 4C) may be also explained by more extensive Arctic sea ice during the period inferred by relatively low Arctic Paleoclimate Index (Fig. 4E), thus suggesting an additional forcing of sea ice or cryosphere (Lachniet et al., 2017).

In contrast, the cave $\delta^{18}O_c$ records from the west-central Asia, Asian and South American Monsoon systems, as well as atmosphere methane (CH_4) follow summer insolation (Cruz et al., 2005; Cheng et al., 2012, 2013b, 2016a, 2016b). Previously, Cheng et al. (2016a) demonstrated a prominent precession cycle from a long Asian Monsoon $\delta^{18}O_c$ record spanning the past 640 kyr, which is in-phase with July insolation. Furthermore, a number of cave $\delta^{18}O_c$ records from South America demonstrate that variations in the South American Monsoon region track changes in Southern Hemisphere summer insolation on orbital timescale with a strong precession periodicity in-phase with 30°S January insolation (e.g., Cruz et al., 2005; Wang et al., 2007; Cheng et al., 2013b).

4.2. Millennial-scale variability

The most prominent millennial-scale events observed in proxy records appear to be of global extent with the trigger possibly residing in the North Atlantic (e.g., Broecker, 1998), although many other potential triggers have now been proposed, including solar forcing (Braun et al., 2008), stochastic atmospheric forcing (Kleppin et al., 2015), regime shifts in oceanic circulation (Knutti et al., 2004), sea ice/ice shelf fluctuations (Boers et al., 2018), volcanism (Baldini et al., 2015), ice sheet dynamics (Zhang et al., 2014), and Antarctic ice sheet discharge (Bakker et al., 2017). These events, such as the Younger Dryas (YD), North Atlantic ice rafted debris (IRD) and Dansgaard-Oeschger (DO) events, or more broadly including the ice age termination events (Cheng et al., 2016a), have been well characterized with Greenland cold events/North Atlantic IRD events broadly corresponding with Antarctic warming/low-latitude monsoon events (e.g., WAIS Divide Project Members, 2015; Cheng et al., 2016a; Wang et al., 2017; Cheng et al., 2018). BCC records appear to show low $\delta^{18}O_c$ values during major Greenland cold events/North Atlantic IRD events or the corresponding major Antarctic warming events and weak (strong) Asian Monsoons (Fig. 8). If indeed, the amplitudes of millennial-scale $\delta^{18}O_c$ variations in BCC records are rather small or even ambiguous, and thus insufficient to definitely characterize the millennial events (Figs. 4 and 8).

The Cave of the Bells and Fort Stanton cave records from southwestern United States show much larger amplitude $\delta^{18}O_c$ excursions (2–5‰) than those in BCC and other cave records in NA. The southwestern lows correspond to Greenland cold events (e.g., Asmerom et al., 2010; Wagner et al., 2010). But a close look at all cave records available in NA shows that the large millennial variability of cave $\delta^{18}O_c$ values occurred primarily in the south and southwestern United States (Cave of the Bells, Fort Stanton and CWN caves) (Asmerom et al., 2010; Wagner et al., 2010; Feng et al., 2014), while all other cave records at higher latitudes show considerably smaller (∼1–2‰ or less) amplitudes

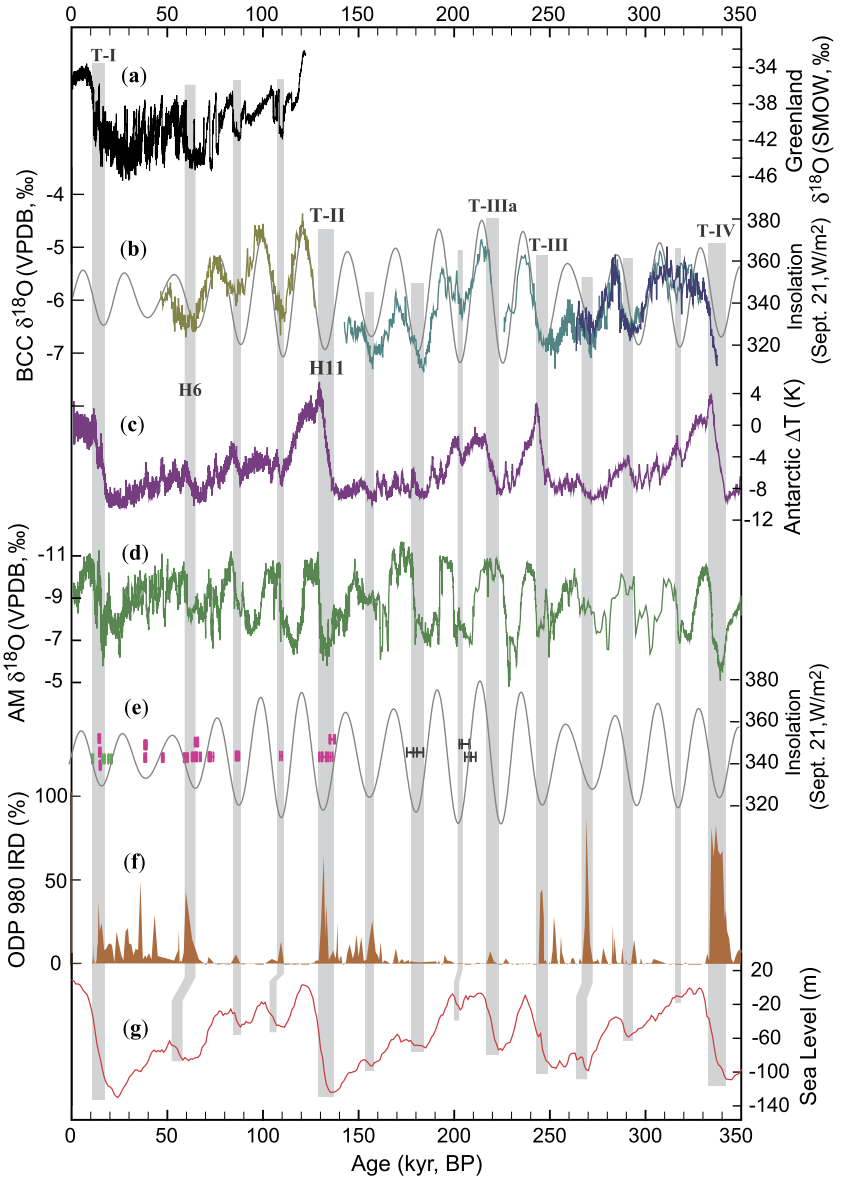

Fig. 8. Comparison of the BCC $\delta^{18}O$ records to additional climate records. **(a)** Greenland ice core (NGRIP) $\delta^{18}O$ record (Wolff et al., 2010). **(b)** BCC records (this study) using color scheme in Fig. 4 and September 21 insolation (grey, Laskar et al., 2004). **(c)** Antarctic temperature anomaly (dark purple, Jouzel et al., 2007). **(d)** Composite Asian Monsoon record (Cheng et al., 2016a). **(e)** North Atlantic marine core (ODP 980) ice rafted debris (IRD) record (dark orange, McManus et al., 1999) and sea level record (red, Spratt and Lisiecki, 2016). Gray bars, corresponding to Greenland cooling, Antarctic warming, weak Asian Monsoon, North Atlantic IRD, and sea level rising events, mark the prominent millennial-scale events.

of the same sign, including McLean and Moaning (Oster et al., 2014, 2015), Oregon cave (OCNM) (Ersek et al., 2012), Lehman, Leviathan and Pinnacle (Lachniet et al., 2014), Crevice (Dorale et al., 1998), and BCC caves. In contrast, a speleothem $\delta^{18}O_c$ dataset from a further north cave (Spring Valley Cave) show the millennial variability in an opposite sign to aforementioned cave records (Nissen et al., 2016).

Asmerom et al. (2010) proposed a mechanism to interpret the large-amplitude millennial events in their Fort Stanton record during the last glacial period: during warm episodes, the pole-to-Equator temperature gradient decreases, shifting the polar jet stream further north, and vice versa (Fig. 1). To first order, this would then change the moisture trajectory/source in the southern-southwestern United States, reducing (during warm mode) Pacific moisture characterized with lighter $\delta^{18}O$, and thus resulting in the observed heavier $\delta^{18}O$ excursion in cave records in the region. The opposite would happen during cold swings (Fig. 1). Contrastingly, during warm (cold) episodes, the polar jet-stream would expect to bring in more (less) Pacific moisture to Spring Valley Cave site in northern United States and resulting in a lighter (heavier) $\delta^{18}O_c$ values as observed in the cave record. This mechanism may explain the lower amplitude $\delta^{18}O_c$ variations during the millennial events as observed in BCC and other cave records in adjacent regions, such as Crevice Cave (CV in Fig. 1). This is because geographically these caves locate along a transition area between aforementioned two different regimes at north and south respectively (Fig. 1). As such the Pacific component of $\delta^{18}O_p$ in these cave sites might not change dramatically during the climate swing between warm and cold modes on millennial-scale, thus dampening the signals from millennial events. In short, recent cave data appear to reinforce the previously proposed mechanism (Asmerom et al., 2010; Lachniet et al., 2017) that the polar jet shifts northward (southward) during warm (cold) climate mode predominantly control the climate variation on millennial-scale across NA (Fig. 1). Mechanistically, this interpretation is in line with a recent hypothesis that the cryospheric forcing (high-latitude sea ice and snow cover) is

one of important drivers of NA paleoclimate through steering of the westerly and storm track (Lachniet et al., 2017).

5. Conclusions

In this study, we present the longest high-precision, well-dated paleoclimate record from eastern NA. The speleothem record spans the last three glacial-interglacial cycles (335–45 kyr ago) and records eastern NA climates responding on orbital time scales to the ice-volume forcing with a significant lag to NH summer insolation (~5 kyr) at the precession band. This fact contrasts with the 'early' (in-phase) responses seen in low-latitude monsoonal records from Asia and South America. Additionally, the unusually low $\delta^{18}O_c$ values also occurred when the global ice-volume was intermediate, which could be casually linked to changes in SST in NE GoM and/or northern high-latitude cryosphere forcing. The BCC $\delta^{18}O_c$ time series have very low amplitude variations on millennial-scale compared to speleothem records from the southwestern United States, so millennial events are only weakly expressed in the BCC $\delta^{18}O_c$ record. We note that this places new constraints on models of Pleistocene climates and affords an opportunity to better interpret shorter or less well-dated records.

Author contributions

G.S., H.C., R.L.E. and B.H. designed the research and experiments. H.C. and G.S. led the writing and revision of the manuscript. G.S. did the fieldwork and collected the samples. H.C., R.L.E., B.H., and Y.T. did the ^{230}Th dating work. H.R. and Y.T., Y.N. and H.C. did oxygen isotope measurements. L.Y., A.S., H.L., X.L. and H.C. did statistical and moisture trajectory analyses. All authors discussed the results and provided input on the manuscript.

Acknowledgements

This work is supported by grants from National Natural Science Foundation of China to H.C. (NSFC 41888101 and 41731174) and US National Science Foundation to R.L.E. and H.C. (1702816).

Appendix A. Supplementary material

Supplementary material related to this article can be found online at https://doi.org/10.1016/j.epsl.2019.06.029.

References

An, Z., Clemens, S.C., Shen, J., Qiang, X., Jin, Z., Sun, Y., Prell, W.L., Luo, J., Wang, S., Xu, H., Cai, Y., Zhou, W., Liu, X., Liu, W., Shi, Z., Yan, L., Xiao, X., Chang, H., Wu, F., Ai, L., Lu, F., 2011. Glacial-interglacial Indian summer monsoon dynamics. Science 333, 719–723.

Asmerom, Y., Polyak, V.J., Burns, S.J., 2010. Variable winter moisture in the southwestern United States linked to rapid glacial climate shifts. Nat. Geosci. 3, 114–117.

Bakker, P., Clark, P.U., Golledge, N.R., Schmittner, A., Weber, M.E., 2017. Centennial-scale Holocene climate variations amplified by Antarctic Ice Sheet discharge. Nature 541, 72–76.

Baldini, J.U.L., Brown, R.J., McElwaine, J.N., 2015. Was millennial scale climate change during the Last Glacial triggered by explosive volcanism? Sci. Rep. 5, 17442.

Bereiter, B., Eggleston, S., Schmitt, J., Nehrbass-Ahles, C., Stocker, T.F., Fischer, H., Kipfstuhl, S., Chappellaz, J., 2015. Revision of the EPICA Dome C CO_2 record from 800 to 600 kyr before present. Geophys. Res. Lett. 42, 542–549.

Blaauw, M., 2010. Methods and code for 'classical' age-modelling of radiocarbon sequences. Quat. Geochronol. 5, 512–518.

Boers, N., Ghil, M., Rousseau, D.-D., 2018. Ocean circulation, ice shelf, and sea ice interactions explain Dansgaard–Oeschger cycles. Proc. Natl. Acad. Sci. USA 115 (47), E11005–E11014.

Braun, H., Ditlevsen, P., Chialvo, D.R., 2008. Solar forced Dansgaard-Oeschger events and their phase relation with solar proxies. Geophys. Res. Lett. 35, L06703.

Broecker, W.S., 1998. Paleocean circulation during the Last Deglaciation: a bipolar seesaw? Paleoceanography 13, 119–121.

Cheng, H., Zhang, P.Z., Spötl, C., Edwards, R.L., Cai, Y.J., Zhang, D.Z., Sang, W.C., Tan, M., An, Z.S., 2012. The climatic cyclicity in semiarid-arid central Asia over the past 500,000 years. Geophys. Res. Lett. 39.

Cheng, H., Edwards, R.L., Shen, C.-C., Polyak, V.J., Asmerom, Y., Woodhead, J., Hellstrom, J., Wang, Y., Kong, X., Spötl, C., Wang, X., Calvin Alexander, E., 2013a. Improvements in ^{230}Th dating, ^{230}Th and ^{234}U half-life values, and U–Th isotopic measurements by multi-collector inductively coupled plasma mass spectrometry. Earth Planet. Sci. Lett. 371–372, 82–91.

Cheng, H., Sinha, A., Cruz, F.W., Wang, X., Edwards, R.L., d'Horta, F.M., Ribas, C.C., Vuille, M., Stott, L.D., Auler, A.S., 2013b. Climate change patterns in Amazonia and biodiversity. Nat. Commun. 4, 1411.

Cheng, H., Edwards, R.L., Sinha, A., Spötl, C., Yi, L., Chen, S., Kelly, M., Kathayat, G., Wang, X., Li, X., Kong, X., Wang, Y., Ning, Y., Zhang, H., 2016a. The Asian monsoon over the past 640,000 years and ice age terminations. Nature 534, 640–646.

Cheng, H., Spötl, C., Breitenbach, S.F.M., Sinha, A., Wassenburg, J.A., Jochum, K.P., Scholz, D., Li, X., Yi, L., Peng, Y., Lv, Y., Zhang, P., Votintseva, A., Loginov, V., Ning, Y., Kathayat, G., Edwards, R.L., 2016b. Climate variations of Central Asia on orbital to millennial timescales. Sci. Rep. 6, 36975.

Cheng, H., Edwards, R.L., Southon, J., Matsumoto, K., Feinberg, M.J., Sinha, A., Zhou, W.J., Li, H.Y., Li, X.L., Xu, Y., Chen, S.T., Tan, M., Wang, Q., Wang, Y.J., Ning, Y.F., 2018. Atmospheric $^{14}C/^{12}C$ changes during the last glacial period from Hulu Cave. Science 362, 1293–1297.

COHMAP Members, 1988. Climatic changes of the last 18,000 years: observations and model simulations. Science 241, 1043–1052.

Cruz, F.W., Burns, S.J., Karmann, I., Sharp, W.D., Vuille, M., Cardoso, A.O., Ferrari, J.A., Silva Dias, P.L., Viana, O., 2005. Insolation-driven changes in atmospheric circulation over the past 116,000 years in subtropical Brazil. Nature 434, 63–66.

Dorale, J.A., Edwards, R.L., Ito, E., González, L.A., 1998. Climate and vegetation history of the Midcontinent from 75 to 25 ka: a speleothem record from Crevice Cave, Missouri, USA. Science 282, 1871–1874.

Draxler, R.R., Hess, G.D., 1998. An overview of the hysplit-4 modeling system for trajectories. Aust. Meteorol. Mag. 47, 295–308.

Edwards, R.L., Chen, J.H., Ku, T.-L., Wasserburg, G.J., 1987. Precise timing of the last interglacial period from mass spectrometric determination of thorium-230 in corals. Science 236, 1547–1553.

Ersek, V., Clark, P.U., Mix, A.C., Cheng, H., Edwards, R.L., 2012. Holocene winter climate variability in mid-latitude western North America. Nat. Commun. 3, 1219.

Feng, W., Hardt, B.F., Banner, J.L., Meyer, K.J., James, E.W., Musgrove, M., Edwards, R.L., Cheng, H., Min, A., 2014. Changing amounts and sources of moisture in the U.S. southwest since the Last Glacial Maximum in response to global climate change. Earth Planet. Sci. Lett. 401, 47–56.

Grayson, D., 2011. The Great Basin: A Natural Prehistory. University of California Press.

Hardt, B., Rowe, H.D., Springer, G.S., Cheng, H., Edwards, R.L., 2010. The seasonality of east central North American precipitation based on three coeval Holocene speleothems from southern West Virginia. Earth Planet. Sci. Lett. 295, 342–348.

Hendy, C.H., 1971. The isotopic geochemistry of speleothems, I: the calculation of the effects of different modes of formation on the isotopic composition of speleothems and their applicability as palaeoclimatic indicators. Geochim. Cosmochim. Acta 35, 801–824.

Howell, P., Pisias, N., Ballance, J., Baughman, J., Ochs, L., 2006. ARAND Time-Series Analysis Software. Brown University, Providence, RI.

IAEA/WMO, 2006. Global Network of Isotopes in Precipitation.

Imbrie, J., Hays, J.D., Martinson, D.G., McIntyre, A., Mix, A.C., Morley, J.J., Pisias, N.G., Prell, W.L., Shackleton, N., 1984. The orbital theory of Pleistocene climate: support from a revised chronology of the marine $\delta^{18}O$ record. In: Berger, A.L. (Ed.), Milankovitch and Climate, Part I. D. Reidel Publishing Company, pp. 269–305.

Jouzel, J., Masson-Delmotte, V., Cattani, O., Dreyfus, G., Falourd, S., Hoffmann, G., Minster, B., Nouet, J., Barnola, J.M., Chappellaz, J., Fischer, H., Gallet, J.C., Johnsen, S., Leuenberger, M., Loulergue, L., Luethi, D., Oerter, H., Parrenin, F., Raisbeck, G., Raynaud, D., Schilt, A., Schwander, J., Selmo, E., Souchez, R., Spahni, R., Stauffer, B., Steffensen, J.P., Stenni, B., Stocker, T.F., Tison, J.L., Werner, M., Wolff, E.W., 2007. Orbital and Millennial Antarctic climate variability over the past 800,000 years. Science 317, 793–796.

Kim, S.-T., O'Neil, J.R., 1997. Equilibrium and nonequilibrium oxygen isotope effects in synthetic carbonates. Geochim. Cosmochim. Acta 61, 3461–3475.

Kleppin, H., Jochum, M., Otto-Bliesner, B., Shields, C.A., Yeager, S., 2015. Stochastic atmospheric forcing as a cause of Greenland climate transitions. J. Climate 28, 7741–7763.

Knutti, R., Fluckiger, J., Stocker, T.F., Timmermann, A., 2004. Strong hemispheric coupling of glacial climate through freshwater discharge and ocean circulation. Nature 430, 851–856.

Lachniet, M.S., Asmerom, Y., Polyak, V., 2011. Deglacial paleoclimate in the southwestern United States: an abrupt 18.6 ka cold event and evidence for a North Atlantic forcing of Termination I. Quat. Sci. Rev. 30, 3803–3811.

Lachniet, M.S., Asmerom, Y., Polyak, V., Denniston, R., 2017. Arctic cryosphere and Milankovitch forcing of Great Basin paleoclimate. Sci. Rep. 7, 12955.

Lachniet, M.S., Denniston, R.F., Asmerom, Y., Polyak, V.J., 2014. Orbital control of western North America atmospheric circulation and climate over two glacial cycles. Nat. Commun. 5, 3805.

Laskar, J., Robutel, P., Joutel, F., Gastineau, M., Correia, A.C.M., Levrard, B., 2004. A long-term numerical solution for the insolation quantities of the Earth. Astron. Astrophys. 428, 261–285.
Marzen, R.E., DeNinno, L.H., Cronin, T.M., 2016. Calcareous microfossil-based orbital cyclostratigraphy in the Arctic Ocean. Quat. Sci. Rev. 149, 109–121.
McManus, J.F., Oppo, D.W., Cullen, J.L., 1999. A 0.5-million-year record of millennial-scale climate variability in the North Atlantic. Science 283, 971–975.
Moseley, G.E., Edwards, R.L., Wendt, K.A., Cheng, H., Dublyansky, Y., Lu, Y., Boch, R., Spötl, C., 2016. Reconciliation of the Devils Hole climate record with orbital forcing. Science 351, 165–168.
Nissen, J., Edwards, R.L., Alexander Jr., E.C., Mackinney, J.S., Shapiro, D., Dasgupta, S., 2016. Reconstructing Midwestern climate variability during the Late Pleistocene. In: GSA Meeting. Denver, Colorado, USA. No: 252-8.
Nürnberg, D., Ziegler, M., Karas, C., Tiedemann, R., Schmidt, M.W., 2008. Interacting loop current variability and Mississippi river discharge over the past 400 kyr. Earth Planet. Sci. Lett. 272, 278–289.
Oster, J.L., Montañez, I.P., Mertz-Kraus, R., Sharp, W.D., Stock, G.M., Spero, H.J., Tinsley, J., Zachos, J.C., 2014. Millennial-scale variations in western Sierra Nevada precipitation during the last glacial cycle MIS 4/3 transition. Quat. Res. 82, 236–248.
Oster, J.L., Montañez, I.P., Santare, L.R., Sharp, W.D., Wong, C., Cooper, K.M., 2015. Stalagmite records of hydroclimate in central California during termination 1. Quat. Sci. Rev. 127, 199–214.
Peixóto, J.P., Oort, A.H., 1983. The atmospheric branch of the hydrological cycle and climate. In: Street-Perrott, A., Beran, M., Ratcliffe, R. (Eds.), Variations in the Global Water Budget. Springer Netherlands, Dordrecht, pp. 5–65.
Rozanski, K., Araguás-Araguás, L., Gonfiantini, R., 1993. Isotopic patterns in modern global precipitation. In: Climate Change in Continental Isotopic Records. American Geophysical Union (AGU), pp. 1–36.
Ruddiman, W.F., 2003. Orbital insolation, ice volume, and greenhouse gases. Quat. Sci. Rev. 22, 1597–1629.
Ruddiman, W.F., 2006. Orbital changes and climate. Quat. Sci. Rev. 25, 3092–3112.
Schulz, M., Mudelsee, M., 2002. REDFIT: estimating red-noise spectra directly from unevenly spaced paleoclimatic time series. Comput. Geosci. 28, 421–426.
Spratt, R.M., Lisiecki, L.E., 2016. A Late Pleistocene sea level stack. Clim. Past 12, 1079–1092.
Springer, G.S., Rowe, H.D., Hardt, B., Cheng, H., Edwards, R.L., 2014. East central North America climates during marine isotope stages 3–5. Geophys. Res. Lett., 2014GL059884.
Springer, G.S., Rowe, H.D., Hardt, B., Edwards, R.L., Cheng, H., 2008. Solar forcing of Holocene droughts in a stalagmite record from West Virginia in east-central North America. Geophys. Res. Lett. 35, L17703.
Wagner, J.D.M., Cole, J.E., Beck, J.W., Patchett, P.J., Henderson, G.M., Barnett, H.R., 2010. Moisture variability in the southwestern United States linked to abrupt glacial climate change. Nat. Geosci. 3, 110–113.
WAIS Divide Project Members, Buizert, C., Adrian, B., Ahn, J., Albert, M., Alley, R.B., Baggenstos, D., Bauska, T.K., Bay, R.C., Bencivengo, B.B., Bentley, C.R., Brook, E.J., Chellman, N.J., Clow, G.D., Cole-Dai, J., Conway, H., Cravens, E., Cuffey, K.M., Dunbar, N.W., Edwards, J.S., Fegyveresi, J.M., Ferris, D.G., Fitzpatrick, J.J., Fudge, T.J., Gibson, C.J., Gkinis, V., Goetz, J.J., Gregory, S., Hargreaves, G.M., Iverson, N., Johnson, J.A., Jones, T.R., Kalk, M.L., Kippenhan, M.J., Koffman, B.G., Kreutz, K., Kuhl, T.W., Lebar, D.A., Lee, J.E., Marcott, S.A., Markle, B.R., Maselli, O.J., McConnell, J.R., McGwire, K.C., Mitchell, L.E., Mortensen, N.B., Neff, P.D., Nishiizumi, K., Nunn, R.M., Orsi, A.J., Pasteris, D.R., Pedro, J.B., Pettit, E.C., Buford Price, P., Priscu, J.C., Rhodes, R.H., Rosen, J.L., Schauer, A.J., Schoenemann, S.W., Sendelbach, P.J., Severinghaus, J.P., Shturmakov, A.J., Sigl, M., Slawny, K.R., Souney, J.M., Sowers, T.A., Spencer, M.K., Steig, E.J., Taylor, K.C., Twickler, M.S., Vaughn, B.H., Voigt, D.E., Waddington, E.D., Welten, K.C., Wendricks, A.W., White, J.W.C., Winstrup, M., Wong, G.J., Woodruff, T.E., 2015. Precise interpolar phasing of abrupt climate change during the last ice age. Nature 520, 661–665.
Wang, Y.Q., 2014. MeteoInfo: GIS software for meteorological data visualization and analysis. Meteorol. Appl. 21, 360–368.
Wang, X., Auler, A.S., Edwards, R.L., Cheng, H., Ito, E., Wang, Y., Kong, X., Solheid, M., 2007. Millennial-scale precipitation changes in southern Brazil over the past 90,000 years. Geophys. Res. Lett. 34, L23701.
Wang, X., Edwards, R.L., Auler, A.S., Cheng, H., Kong, X., Wang, Y., Cruz, F.W., Dorale, J.A., Chiang, H.-W., 2017. Hydroclimate changes across the Amazon lowlands over the past 45,000 years. Nature 541, 204–207.
Wang, Y.Q., Zhang, X.Y., Draxler, R.R., 2009. TrajStat: GIS-based software that uses various trajectory statistical analysis methods to identify potential sources from long-term air pollution measurement data. Environ. Model. Softw. 24, 938–939.
Wendt, K.A., Dublyansky, Y.V., Moseley, G.E., Edwards, R.L., Cheng, H., Spötl, C., 2018. Moisture availability in the southwest United States over the last three glacial-interglacial cycles. Sci. Adv. 4, eaau1375.
Winograd, I.J., Landwehr, J.M., Coplen, T.B., Sharp, W.D., Riggs, A.C., Ludwig, K.R., Kolesar, P.T., 2006. Devils Hole, Nevada, δ^{18}O record extended to the mid-Holocene. Quat. Res. 66, 202–212.
Wolff, E.W., Chappellaz, J., Blunier, T., Rasmussen, S.O., Svensson, A., 2010. Millennial-scale variability during the last glacial: the ice core record. Quat. Sci. Rev. 29, 2828–2838.
Yurtsever, Y., 1975. Worldwide Survey of Stable Isotopes in Precipitation. International Atomic Energy Agency, Vienna, Austria.
Zhang, X., Lohmann, G., Knorr, G., Purcell, C., 2014. Abrupt glacial climate shifts controlled by ice sheet changes. Nature 512, 290–294.